IET Image Processing

Research Article

IET Journals
The Institution of Engineering and Technology

Localised rank-ordered differences vector filter for suppression of high-density impulse noise in colour images

ISSN 1751-9659
Received on 21st October 2014
Revised on 9th June 2015
Accepted on 5th July 2015
doi: 10.1049/iet-ipr.2014.0838
www.ietdl.org

Bernardino Roig ✉, *Vicente D. Estruch*

Universidad Politécnica de Valencia, E.P.S. Gandia, C/Paranimf, 1., 46730 Grau de Gandia (Valencia), Spain
✉ *E-mail: broig@mat.upv.es*

Abstract: This research presents a complete study of a new alternating vector filter for the removal of impulsive noise in colour images. The method is based on an impulsive noise detector for greyscale images that has been adapted in a localised manner using geometric information for processing colour images. Based on this statistic, a filtering scheme alternating between the identity and a non-linear vector filter is proposed. A geometric and experimental study was performed to obtain the optimal filter design. Experimental studies show that the proposed technique is simple, easy to implement, robust to noise, and outperforms the classic vector filters, as well as more recent filters.

1 Introduction

Impulsive noise is introduced into digital images during processes of acquisition and transmission. The process of impulsive noise corruption affects only some pixels in an image and leaves the remainder unchanged. The noise usually changes one or more colour components of a pixel and replaces the original values. The most common types of impulsive noise models consider that the impulse is either an extreme value in the range of the signal (fixed-value impulsive noise); or a random value uniformly distributed within the range of the signal (random value impulsive noise).

Consequently, since impulsive noise can be seen as an unusual or unexpected value, methods based on the theory of robust statistics, such as the median filter [1] (MF), or its generalisation to the multichannel case, the vector median filter [2] (VMF), have been widely used to reduce impulsive noise. Vector processing has proved suitable for processing colour images since it takes into account correlation between colour channels in the image [3–5]. Given that the filtering operation in classic filters is performed on each pixel of the image regardless of whether it is noisy or not, the resulting images usually suffer blurred edges and loss of detail; so that the overall quality is significantly degraded. An intuitive idea to solve this problem is proposed that enables switching between applying a pixel filter or not – depending on whether noise is detected or not. This approach preserves the noise-free structures of the image.

Many alternating filter techniques have been proposed to detect impulses. For example, it is possible to perform a cluster analysis around a pixel and detect noisy pixels whose degree of cluster membership is low [6]. Several methods use contours to distinguish between pixels that are noise-free or not [7, 8]. The theory of quaternion rotation can also be employed [9]. Several studies use a fuzzy inference system that takes statistical measures of the pixel and its surroundings as an input [10, 11]. Another method detects noise by the input vector and the distances added to other vectors within the filter window [12]. Another filter evaluates the range of the processed pixels in various orderings [13]. Some techniques use robust estimators [14, 15]. One possible solution uses coefficients weighted with regard to the centre [16], and some methods use similarities based on a vector-based ordering to increase the importance of the considered pixel in the impulsive noise detection process [17, 18]. The concept of peer group is also employed [19, 20]. Some methods use differences between the pixel and its surroundings in the four major directions [21, 22] or in the entire environment [23].

Other adaptive filtering methods have also been proposed – including weighted coefficients [24, 25], fuzzy logic [26, 27] and neuro-fuzzy systems [28]. Further information can be found in revisions in the literature [3, 4].

The window mask size of the filter also plays an important role in finding the most suitable value; larger and smaller windows lead to distortions when the impulse noise ratios are low and high respectively. At higher noise ratios all the signal intensities chosen from a pre-defined neighbourhood can go noisy and the result of the filter from such a noisy region can be an impulse. Bigger window mask is applied to the areas with high level of noise, and smaller window mask is applied to the areas with low level of noise. Thus the non-adaptiveness of the window mask size to density of noise gives an incorrectly chosen impulse substitute [29, 30]. Some adaptive filters started with a smaller window size first, and increase the size until certain conditions are met [31, 32].

The proposed localised detection method checks whether each pixel is noisy or not using a fixed window mask size for all ratio noise intensities. A finite number of subwindows are defined inside which are used to remove impulsive noise while preserving fine details. When a corrupt pixel is detected, the proposed alternating filter performs a non-linear filtering, while pixels free of noise are left unaltered. The VMF, the arithmetic mean filter [33] (AMF), and the Perona–Malik filter [34] (PMF) – as well as non-linear filters – were tested on corrupt pixels. Extensive experiments and geometric studies were performed to analyse the proposed technique, and therefore, the optimal settings for window size, colour vector metric, and parameters.

Section 2 introduces the statistical analysis, and the proposed filter is defined in Section 3. Experimental results are presented in Section 4, and finally, conclusions are offered in Section 5.

2 Localised rank-ordered differences statistic for RGB colour images

This section examines the rank-ordered differences statistic for RGB colour images and an improved statistical algorithm for all impulsive noise densities is then proposed.

2.1 Rank-ordered differences statistic for RGB colour images

For each pixel $\boldsymbol{x}$ an $n \times n$ $\Omega_{\boldsymbol{x}}$ window is centred on $\boldsymbol{x}$, where each $\boldsymbol{y} \in \Omega_{\boldsymbol{x}}$ pixel is represented by a colour RGB vector $(y(1), y(2),$

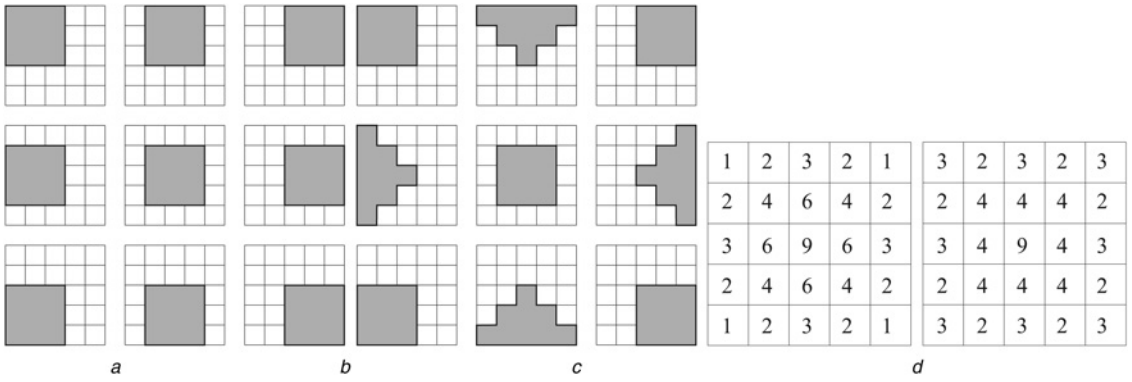

Fig. 1 *Two types of superimposed nine-pixel subwindows. All are within a 5 × 5 window centred on x. In each case, the subwindows are numbered from left- to right-hand side and from top to bottom as* $\Omega_{x,1}, \ldots, \Omega_{x,9}$

a Nine square subwindows of nine pixels
b Nine triangular and square windows of nine pixels. Number of subwindows in which a pixel appears in
c Nine square nine-pixel subwindows
d Nine square and triangular nine-pixel subwindows

$y(3)) \in X^3$ where $X = \{0, 1, \ldots, 255\}$. The distances $d^1_{x,y}$, $d^2_{x,y}$ and $d^\infty_{x,y}$ are defined by the norms L_1 (city-block), L_2 (Euclidean), and L_∞, and the RGB colour space between the colour vectors $\boldsymbol{x}$ and $\boldsymbol{y}$ respectively. $\Omega^0_{\boldsymbol{x}} = \Omega_{\boldsymbol{x}} - \{\boldsymbol{x}\}$ denotes the set of $\boldsymbol{x}$ neighbours in the window. By considering k fixed at $\{1, 2, \infty\}$, the distances $d^k_{x,y}$ are calculated for $\boldsymbol{y} \in \Omega^0_{\boldsymbol{x}}$ and these are ranked in ascending order as

$$d^k_{x,y}(1) \leq d^k_{x,y}(2) \leq \cdots \leq d^k_{x,y}(n^2 - 1) \tag{1}$$

where $d^k_{x,y}(j)$ denotes jth smallest value of the set $\{d^k_{x,y}, \boldsymbol{y} \in \Omega^0_{\boldsymbol{x}}\}, j = 1, \ldots, n^2 - 1$. With the positive integer $m < n^2$, the m-rank ordered difference statistic ROD_m is defined as follows

$$\mathrm{ROD}_m(\boldsymbol{x}) = \sum_{i=1}^{m} d^k_{x,y}(i). \tag{2}$$

The defined ROD statistical algorithm is a generalisation to RGB colour images of ROAD [24] for greyscale images. The ROD_m algorithm gives a measurement of how close a pixel is to its m nearest neighbours in $\Omega^0_{\boldsymbol{x}}$ with reference to the colour RGB vectors. The logic behind this statistical algorithm is that the impulses vary significantly in one or more colour components with respect to most of the neighbouring pixels, while most noise-free pixels are similar to their surroundings. Therefore, noise-free pixels show a significantly lower value in the ROD_m statistical algorithm than pixels corrupted with impulsive noise.

2.2 *New localised rank-ordered differences statistic*

Since it has already been studied [35], the ROD_m statistic behaves in an ideal way when the environment $\Omega_{\boldsymbol{x}}$ is a 3 × 3 window ($n = 3$) in low noise cases. On the other hand, when the noise increases, there is no enough information in a 3 × 3 window and a 5 × 5 window ($n = 5$) is the ideal one for the environment $\Omega_{\boldsymbol{x}}$. Now then, on having considered 5 × 5 windows, definition gets lost in the details and in borders with few resolution.

To develop a robust statistic for the amount of noise and retain definition in details a new statistic termed *localised rank-ordered differences* (LROD) is proposed. A 5 × 5 window centred on the pixel for the $\Omega_{\boldsymbol{x}}$ surrounding is considered for its definition. Two types of superimposed nine-pixel subwindows that include the centre pixel as shown in Figs. 1*a* and *b* are defined.

Figs. 1*c* and *d* shows the number of times that a pixel appears in the various subwindows. It can be seen that in the nine square nine-pixel windows a Gaussian distribution is followed with respect to the central pixel ($\sigma \simeq 1.2$). However, in the nine square and triangular nine-pixel subwindows, a linear distribution seems to be followed in which the diagonal and cross directions are prioritised. As giving more weight to some directions than others is *a priori* arbitrary, the Gaussian distribution is chosen for weighting each pixel. Although the nine square subwindows of nine pixels are chosen, the experimental results performed reveal no significant differences between using nine square subwindows, or the nine square and triangular subwindows.

In Fig. 2*a* we show four key detail cases. Let us assume for simplicity that the detail is grey while the surroundings are white. From Fig. 2*a* it is easy to see that there are three subwindows with six (or five) detail pixels. Then, if the central pixel is not noisy, there must have at least three subwindows with five (or four) pixels similar to it, one less if one of them is corrupted. The parameter m indicates the number of pixels we can find similar to the central pixel in at least three subwindows. Its value cannot be greater than 4 (or 3).

In the LROD_m statistic, the ROD_m is first calculated (as defined in the previous section) for each of the nine square 3 × 3 subwindows considered in $\Omega_{\boldsymbol{x}}$. At least three of the nine subwindows are then required to have a ROD_m small enough to consider the central pixel $\boldsymbol{x}$ as noise-free. As it has been discussed in the previous paragraph, this enables the detection of corners because at least three of the nine sub-windows have enough pixels similar to the central pixel within the considered corner. This definition also enables the detection of fine lines of at least two pixels in width as at least three of the nine subwindows have enough pixels similar to the central pixel under consideration.

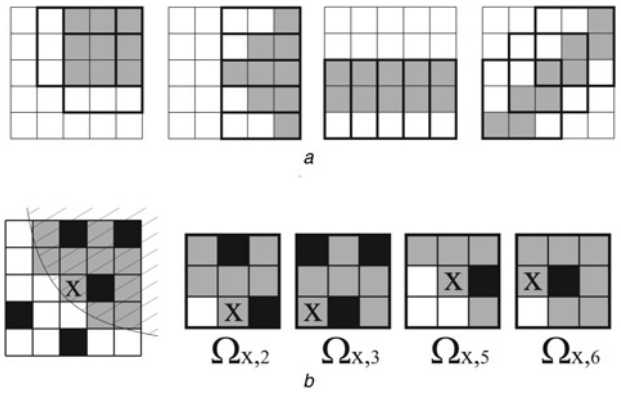

Fig. 2 *Detail cases*

a Three subwindows with six pixels in two corner detail cases and with five pixels in two fine line detail cases
b Round corner detail example with 20% of impulsive noise where $\Omega_{\boldsymbol{x}}$ has more than three subwindows ($\Omega_{x,2}$, $\Omega_{x,3}$, $\Omega_{x,5}$ and $\Omega_{x,6}$) with at least four pixels ($m = 4$) similar to the central pixel $\boldsymbol{x}$

Fig. 2*b* presents an example where the impulsive noise is shown in black. As can be seen, there are four subwindows with at least 3 pixels similar to $\boldsymbol{x}$, thus the ROD_3 statistic is small in at least three subwindows. Therefore, the pixel is classified as not corrupt by LROD filter (LRODF) with $m=3$. In addition, as it is shown in the same figure, there are four subwindows with at least 4 pixels similar to $\boldsymbol{x}$, hence the ROD_4 statistic is small in at least three subwindows. Therefore, the pixel is classified as not corrupt by LRODF with $m=4$. In this example, there are more than three subwindows verifying the condition of having 3 or 4 pixels similar to $\boldsymbol{x}$, however when the impulsive noise increase or when the limit cases of Fig. 2*a* are considered it is more difficult to achieve more than three subwindows fulfilling this condition. Moreover, if we assume that the central pixel $\boldsymbol{x}$ of this example is also corrupted by noise (black pixel) it is easy to check that there are not any subwindows with at least 3 pixels similar to $\boldsymbol{x}$, and therefore $\boldsymbol{x}$ will be considered a corrupt pixel.

The only drawback to this and other switching filters to remove impulse noise is cases in which a group of noisy pixels is considered as a detail to preserve.

3 Proposed filtering method

The proposed filtering scheme termed LRODF considered in the previous section is performed in two steps. In the first step, the corrupt pixels are detected, while in the second step each pixel marked as corrupt is replaced by the result of a non-linear filter, such as for example, the VMF.

The noise detection process proceeds as follows:

(i) $\Omega_{\boldsymbol{x}}$ is considered as a 5×5 window centred on $\boldsymbol{x}$ as in Fig. 1*a*. Let $\Omega^0_{\boldsymbol{x},j}=\Omega_{\boldsymbol{x},j}-\{\boldsymbol{x}\}$, $j=1,\ldots,9$.
(ii) For each subwindow $\Omega_{\boldsymbol{x},j}$ the distances $d^k_{\boldsymbol{x},\boldsymbol{y}}$ with $k=\infty$ are calculated for all the $\boldsymbol{y}\in\Omega^0_{\boldsymbol{x},j}$ which are ranked in ascending order as in the calculation of ROD_m (see (1)).
(iii) For each subwindow $\Omega_{\boldsymbol{x},j}$ the ROD_m is calculated with $m=4$ (see (2)). If it is less than the predefined tolerance d_{T}, with $d_{\mathrm{T}}=130$, then the $\Omega_{\boldsymbol{x},j}$ subwindow is considered *similar* to the central pixel. Otherwise, it is considered *dissimilar*.
(iv) If the number of subwindows indicated as *similar* to the central pixel is greater than, or equal to, three then the $\boldsymbol{x}$ pixel is marked as *not corrupt*. Otherwise, it is marked as corrupt.

Other values of k and m and d_{T} have been studied in the next section where we see that $k=\infty$ is the best option, $m=3$ with $d_{\mathrm{T}}=75$ is also good for noises below 40% and (5) gives another suboptimal value for d_{T}.

The output of the filtering operation is denoted as $\boldsymbol{y}_{\mathrm{LRODF}}$, the central pixel is denoted $\boldsymbol{x}$, and the VMF output of the non-linear filter is denoted as $\mathrm{VMF}_{\mathrm{out}}$. Other filters can be used such as the AMF over not corrupt pixels, or an iteration of the Perona–Malik non-linear diffusion filter given its proven ability to maintain and improve edges and improve the flow structures [36, 37]. The terms LROD-AMF, and LROD-PMF will be used when using the AMF and PMF filters respectively instead of VMF. There is no blur effect because only the pixels marked as corrupt are replaced. The alternating filter method proceeds as follows

$$\boldsymbol{y}_{\mathrm{LRODF}}=\begin{cases}\boldsymbol{x} & \text{if } \boldsymbol{x} \text{ is non-corrupted}\\ \mathrm{VMF}_{\mathrm{out}} & \text{if } \boldsymbol{x} \text{ is corrupted}\end{cases} \tag{3}$$

Note that for each $\Omega_{\boldsymbol{x}}$ window it is only necessary to calculate and order the distances to the central pixel once. It is then only necessary to consider the distances corresponding to each subwindow. In the following paragraphs, we show that the computational load of rank-ordered differences switching vector filter (RODSF) is, in general, lower than the VMF by comparing the number of computed distances because they are the most expensive from a computational view. Initially, for a 5×5 window, the LRODF detector computes n_1^2-1 distances with $n_1=5$ see (1). In addition, if the pixel is corrupted, the VMF operation has to be computed. This implies the computation of $\left((n_2^2-1)(n_2^2-2)/2\right)$ additional distances when an $n_2\times n_2$ window mask is used in the VMF. The global number of distances computed by LRODF is given by the expression

$$(n_1^2-1)+p'\frac{(n_2^2-1)(n_2^2-2)}{2} \tag{4}$$

where p' denotes the probability that a pixel is considered as corrupt by LRODF. A visual assessment can be made for p', but we can obtain a good approximation defining p' as the ratio between noisy pixels detected with the filter. If the calculated distances are not recomputed at each step in VMF, the number of distances to be evaluated can be reduced from $\mathcal{O}(n_2^4)$ to $\mathcal{O}(n_2^3)$ [5]. We can also reduce this number by reusing the distances computed in the detector step.

In the following cases, we assume that the distances are recomputed at all times. Assuming the used values, $n_1=5$ and $n_2=3$, for an image with 20% of impulsive noise the computed distances for each pixel are similar in LRODF and in VMF to about 29. For lower noises, thanks to (4) it is easy to see that LRODF is computationally cheaper than VMF. For high impulsive noises, bigger values of n_2 are needed [30]. Consider $p=0.50$, $n_1=5$, and $n_2=5$, then 162 distances are computed for each pixel by LRODF and 276 by VMF; hence LRODF is computationally cheaper than VMF. In general, LRODF is cheaper than VMF or, in the worst case, similar to VMF. This is because in (4) the window size for the detector step, n_1, is power to 2, while the window size for the VMF, n_2, is power to 4.

Moreover, (4) also applies to the non-localised filter RODSF [35] with $n_1=3$. In the previous cases the number of computed distances are 14 and 146 for $n_2=3$ and $p=0.2$, and for $n_2=5$ and $p=0.5$ respectively. So, assuming that the distances are always recomputed in each pixel, in the detector step the localised filter, LRODF, adds $5^2-1=24$ distances to calculate to the number of computed distances in the filtering operation

$$p'\frac{(n_2^2-1)(n_2^2-2)}{2}$$

while the non-localised version, RODSF, adds $3^2-1=8$.

4 Experimental study

A study was made using various options for the parameters within the proposed filter scheme to obtain an optimal design for the filter. The Lenna, House, Peppers, and Parrot zoomed images of 90×90, 70×70, 50×50, and 90×90 window sizes respectively were used for this study to better appreciate the performance differences (Fig. 3). The images are distorted using various densities of impulsive noise [5]. Three indicators were used to evaluate the performance achieved: normalised colour difference (NCD) [5], the peak signal-to-noise ratio (PSNR) [5], and a more advanced method called colour multiscale structural similarity index (CMSSIM) [38]. NCD was used since it correlates well with human perception, PSNR measures the ability to reduce noise, and CMSSIM is intended to take into account three main factors in the similarity to better agree with perceptual evaluation: luminance, contrast and structure similarity.

First, a comparison was made of the developed localised filter, the LRODF, with the non-localised version of the filter, the RODSF [35]. For tolerance, the optimal d_{T} values obtained experimentally for each case with the metric L_∞ were used. Figs. 4*a* and *b* shows the NCD and PSNR values obtained by filtering the Lenna image contaminated with various noise densities. It can be seen that LRODF with $m=3$ and $m=4$ behave similarly to RODSF for noise densities below 10% and that its performance is better than RODSF for the others noise densities. Similar results were obtained with the other images and with the CMSSIM index. This

IET Image Process., 2016, Vol. 10, Iss. 1, pp. 24–33

Fig. 3 *Lenna, house, peppers and parrots zoomed images from left- to right-hand side*

confirms that the filter is robust with variations in impulsive noise and improves RODSF – thus offering a competitive performance when compared with other vector filters [35].

We then explored what is the most appropriate value of m in {2, 3, 4}, given that as seen in Section 2.2, m must be less than 5 to preserve fine details. Figs. 4*c* and *d* shows the behaviour in terms of NCD and PSNR for various values of m for the Lenna image and for the optimal value of d_T with the metric L_∞. The worst results are obtained for $m = 2$ given that in LRODF it does not increase robustness and, in consequence, the efficiency of the filter diminishes as the noise increases. Options $m = 3$ and $m = 4$ give better results for low and high levels of impulsive noise. Similar results were obtained for the other images and the CMSSIM index.

The next step was to determine the most appropriate distance criterion between the norms L_1, L_2, and L_∞ in the colour vector space. Figs. 5*a* and *b* shows the behaviour of NCD and PSNR for the various metrics for an optimal tolerance d_T with $m = 4$ for the Lenna image. The best behaviour is achieved with L_∞. Similar

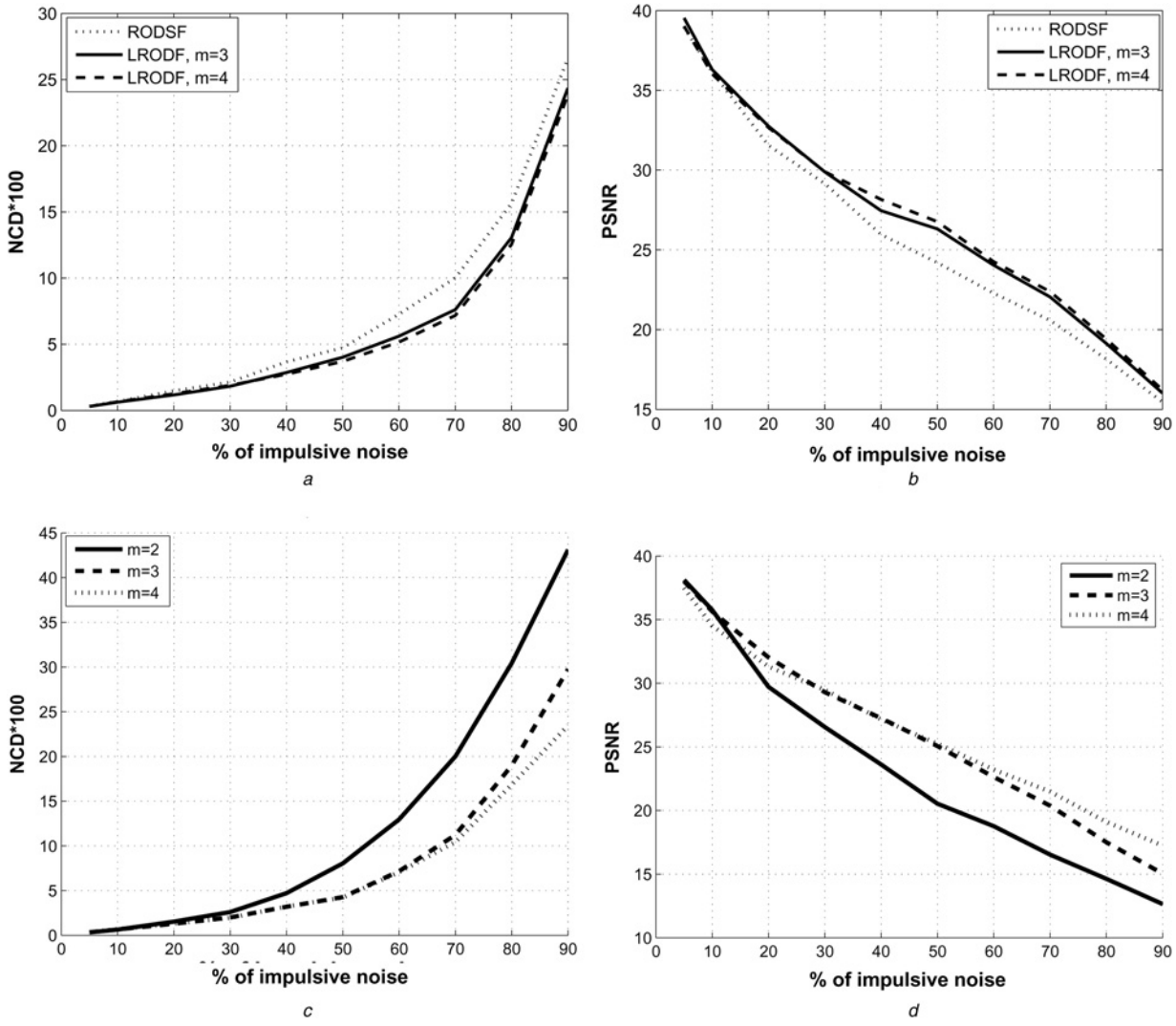

Fig. 4 *Behaviour of LRODF compared to RODSF using the metric L∞ when filtering the Lenna image contaminated with impulsive noise for LRODF with m = 3 (solid line), LRODF with m = 4 (dashed line) and RODSF with n = 3 (dotted line) in terms of*

a NCD
b PSNR
Results of the LRODF with the metric L∞ used in the filtering of the Lenna image contaminated with impulsive noise for various values of m: m = 2 (solid line), m = 3 (dashed line), m = 4 (dotted line) in terms of
c NCD
d PSNR

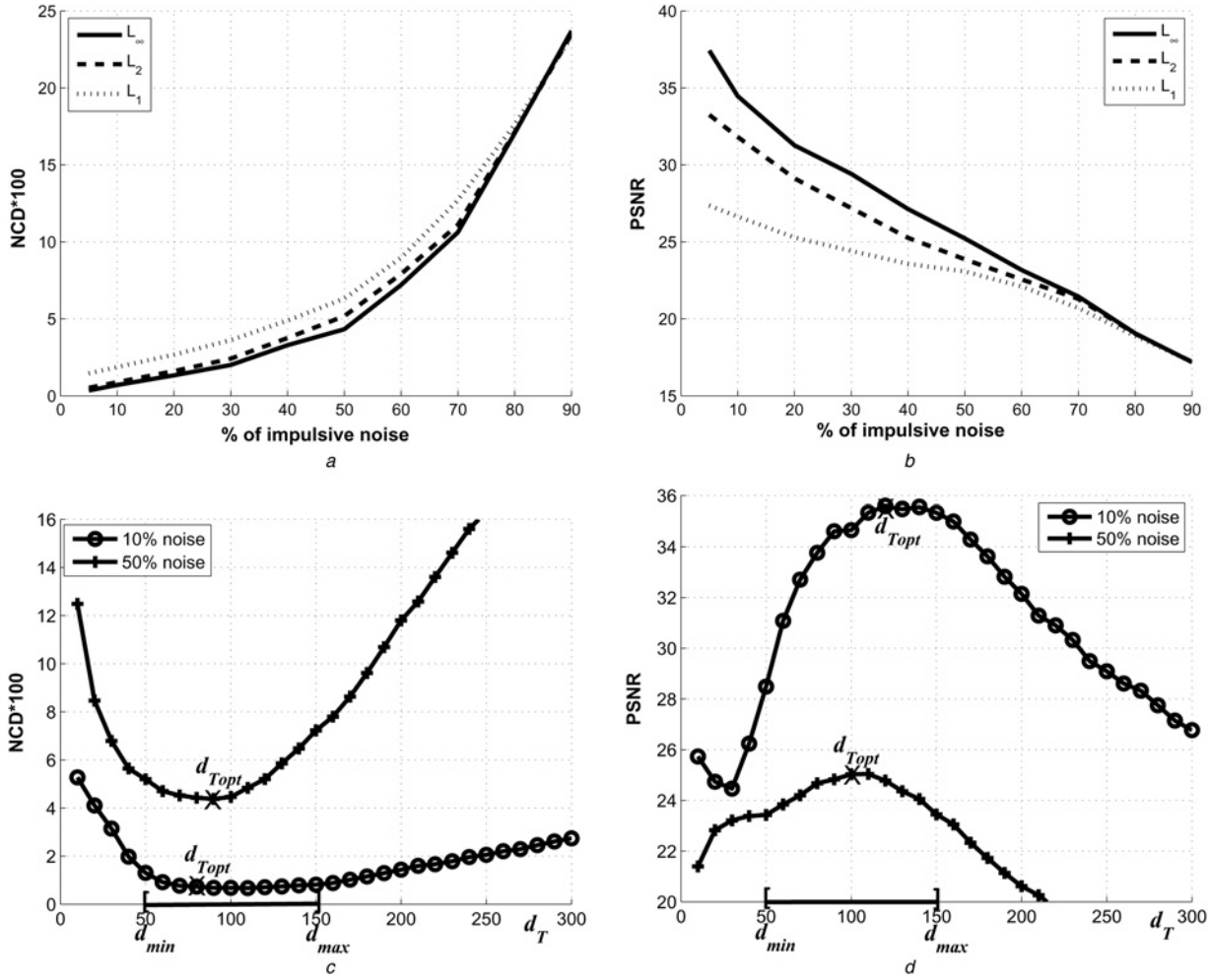

Fig. 5 *Results of the LRODF with m = 4 used in the filtering of the Lenna image contaminated with impulsive noise for various metrics: L∞ (solid line), L2 (dashed line), L1 (dotted line) of*

a NCD
b PSNR
Results of the LROD-AMF when m = 3 in function of the tolerance dT for the Lenna image with 10% (°) and 50% (+) of impulsive noise with L∞ of
c NCD
d PSNR

results are obtained with $m = 3$, the other images and the CMSSIM index. This is probably because the L_∞ metric is the worst case metric in the sense that the value given by the metric corresponds to the maximum difference observed among the colour vector components. Given that the impulsive noise in a colour vector can be easily detected by a simple examination of the maximum difference, it is reasonable that the best method of detecting impulsive noise is associated with the L_∞ metric.

Finally, the approximate value of the d_T tolerance parameter can be established by an analysis of the dependence of the LRODF results with respect to d_T when the L_∞ metric is used. Figs. 5*c* and *d* shows several results for various densities of noise for LROD-AMF and the Lenna image. Similar results are obtained with $m = 4$, other images, the CMSSIM index, and non-linear filters. These results indicate that the optimal value d_{Topt} for d_T is usually in the range $[d_{min}, d_{max}] = [50, 150]$ when $m = 3$, and in

Table 1 Performance comparison in terms of NCD (10^{-2}) using the Lenna and House detail images contaminated with different probabilities *p* of impulsive noise

p	Lenna					House				
	0.1	0.2	0.4	0.6	0.8	0.1	0.2	0.4	0.6	0.8
VMF [2]	2.87	3.07	3.75	5.55	*12.63*	2.96	3.07	3.59	*5.16*	**13.30**
IPGSAMF [19]	2.30	3.90	5.62	10.13	19.30	3.24	6.21	7.76	11.78	23.59
FIVF [17]	0.94	1.75	4.10	10.14	25.94	0.60	1.15	2.79	8.76	26.72
AVMF [12]	0.94	2.10	7.46	17.38	34.96	0.77	1.58	6.27	18.26	37.78
PGSAMF [20]	0.79	1.85	5.57	13.95	33.29	0.58	1.28	4.51	13.18	39.16
RODSF [35]	0.69	1.40	3.37	6.98	*15.80*	*0.46*	1.07	2.49	5.58	*15.87*
LRODF$_{m=3}$	**0.46**	**0.85**	**2.16**	**4.93**	*13.43*	*0.48*	*0.88*	*2.37*	*5.43*	16.77
LROD-AMF$_{m=3}$	*0.51*	*0.90*	*2.31*	*6.28*	19.16	0.53	0.90	2.55	6.59	25.20
LROD-PMF$_{m=3}$	*0.50*	*0.87*	*2.26*	*6.15*	*18.99*	0.52	*0.87*	2.48	6.45	24.98
LRODF$_{m=4}$	*0.65*	*1.26*	*2.74*	*5.15*	**12.61**	**0.45**	**0.86**	*1.87*	**4.42**	*13.33*
LROD-AMF$_{m=4}$	0.67	1.31	3.21	7.20	17.04	0.51	0.90	*1.82*	5.67	16.81
LROD-PMF$_{m=4}$	0.66	1.29	3.16	7.04	16.84	*0.50*	*0.87*	**1.76**	*5.52*	*16.48*

IET Image Process., 2016, Vol. 10, Iss. 1, pp. 24–33

Table 2 Performance comparison in terms of PSNR using the Lenna and House detail images contaminated with different probabilities p of impulsive noise

p	Lenna					House				
	0.1	0.2	0.4	0.6	0.8	0.1	0.2	0.4	0.6	0.8
VMF [2]	29.37	28.74	27.04	*24.17*	**19.40**	32.30	31.71	*29.62*	**24.91**	**19.34**
IPGSAMF [19]	28.62	26.49	24.32	20.93	16.03	26.55	24.82	23.95	21.51	15.58
FIVF [17]	32.64	29.94	25.39	20.34	15.11	37.09	33.91	27.28	20.79	15.30
AVMF [12]	32.34	28.97	22.02	17.48	13.59	35.00	30.81	23.09	17.58	13.74
PGSAMF [20]	33.27	28.87	22.95	18.43	13.79	37.77	32.31	24.27	18.65	13.19
RODSF [35]	35.55	32.08	27.10	23.05	18.43	38.50	34.33	28.85	*23.83*	18.43
LRODF$_{m=3}$	*38.77*	*35.62*	**28.75**	*23.90*	18.88	*38.69*	*35.63*	28.33	23.50	17.71
LROD-AMF$_{m=3}$	*38.70*	*35.43*	*28.07*	22.69	17.48	38.30	35.02	27.78	22.66	15.99
LROD-PMF$_{m=3}$	**39.08**	**35.71**	*28.15*	22.74	17.50	38.62	35.22	27.85	22.72	16.01
LRODF$_{m=4}$	*36.02*	*32.67*	*28.15*	**24.29**	*19.37*	*38.72*	*35.58*	**31.31**	*24.91*	*19.27*
LROD-AMF$_{m=4}$	35.79	32.29	27.58	23.17	*19.06*	*38.76*	*35.41*	*30.42*	*23.83*	*19.13*
LROD-PMF$_{m=4}$	35.79	32.29	27.58	*23.22*	*19.11*	**39.11**	**35.65**	*30.56*	*23.93*	*19.23*

Table 3 Performance comparison in terms of CMSSIM (10^{-1}) using the Lenna and House detail images contaminated with different probabilities p of impulsive noise

p	Lenna					House				
	0.1	0.2	0.4	0.6	0.8	0.1	0.2	0.4	0.6	0.8
VMF [2]	9.83	9.72	*9.42*	*8.44*	**5.72**	9.88	9.89	*9.70*	*8.72*	*5.73*
IPGSAMF [19]	8.75	7.82	6.25	5.20	3.29	8.45	7.05	6.31	4.92	3.40
FIVF [17]	9.67	9.41	8.47	5.90	2.76	9.90	9.87	9.32	6.76	2.64
AVMF [12]	9.83	9.34	7.07	3.83	1.92	9.91	9.62	7.48	4.04	2.10
PGSAMF [20]	9.80	9.40	7.41	4.35	1.84	9.94	9.71	8.13	5.29	1.81
RODSF [35]	9.89	*9.76*	*8.99*	*7.38*	*4.72*	*9.98*	9.90	9.50	8.15	*4.74*
LRODF$_{m=3}$	**9.99**	**9.85**	*9.25*	*7.77*	*4.82*	*9.99*	*9.99*	9.63	*8.45*	*4.92*
LROD-AMF$_{m=3}$	*9.88*	*9.74*	8.81	6.62	3.01	*9.99*	*9.99*	9.63	8.07	3.00
LROD-PMF$_{m=3}$	*9.88*	*9.74*	8.85	6.67	2.99	*9.99*	*9.98*	9.62	8.07	2.99
LRODF$_{m=4}$	*9.91*	*9.79*	**9.50**	**8.48**	*5.71*	**10.00**	**10.00**	*9.86*	**8.83**	**5.84**
LROD-AMF$_{m=4}$	9.87	9.68	8.84	7.15	3.42	*9.99*	*9.99*	*9.89*	8.21	3.69
LROD-PMF$_{m=4}$	9.87	9.70	8.88	7.19	3.45	**10.00**	**10.00**	**9.94**	*8.26*	3.75

Table 4 Performance comparison in terms of NCD (10^{-2}) using the Peppers and Parrots detail images contaminated with different probabilities p of impulsive noise

p	Peppers					Parrots				
	0.1	0.2	0.4	0.6	0.8	0.1	0.2	0.4	0.6	0.8
VMF [2]	2.78	2.91	3.78	5.58	*11.97*	3.66	3.96	*4.81*	*7.92*	*15.79*
IPGSAMF [19]	1.90	3.45	7.09	11.67	19.51	3.47	5.50	8.93	14.97	26.97
FIVF [17]	0.93	1.38	4.25	9.57	21.94	2.19	3.04	5.82	13.41	29.38
AVMF [12]	0.71	1.81	7.03	15.77	29.32	1.67	3.14	9.15	21.42	37.18
PGSAMF [20]	0.93	1.40	4.97	13.79	30.16	2.11	3.66	7.98	19.65	36.95
RODSF [35]	0.66	1.07	3.44	*6.83*	*13.66*	1.90	2.85	5.14	10.52	19.89
LRODSF$_{m=3}$	*0.58*	*0.98*	*2.77*	*5.77*	*13.03*	**1.23**	**2.16**	*3.97*	*8.07*	*16.52*
LROD-AMF$_{m=3}$	*0.56*	*0.93*	*2.99*	8.21	17.51	*1.41*	*2.50*	4.92	9.82	20.79
LROD-PMF$_{m=3}$	**0.56**	**0.92**	*2.96*	8.14	17.40	*1.41*	*2.48*	4.90	9.72	20.60
LRODF$_{m=4}$	0.61	1.02	**2.67**	**5.22**	**11.96**	*1.45*	*2.37*	**3.94**	**7.54**	**15.73**
LROD-AMF$_{m=4}$	*0.60*	1.00	3.04	7.27	15.00	1.77	2.87	4.83	9.16	*18.40*
LROD-PMF$_{m=4}$	*0.59*	*0.99*	3.01	*7.19*	14.86	1.77	2.85	*4.78*	*9.03*	18.82

Table 5 Performance comparison in terms of PSNR using the Peppers and Parrots detail images contaminated with different probabilities p of impulsive noise

p	Peppers					Parrots				
	0.1	0.2	0.4	0.6	0.8	0.1	0.2	0.4	0.6	0.8
VMF [2]	28.14	27.57	25.81	*22.81*	*18.88*	23.18	22.71	*21.87*	*19.42*	*16.84*
IPGSAMF [19]	27.42	25.98	22.53	19.67	15.79	20.28	19.87	17.40	14.97	12.74
FIVF [17]	31.18	29.98	24.65	19.45	15.16	23.53	22.23	19.94	16.89	13.86
AVMF [12]	31.82	28.66	21.66	17.28	13.78	25.67	24.06	20.24	16.18	13.30
PGSAMF [20]	30.35	29.24	23.25	17.39	13.40	22.57	21.39	18.27	15.29	12.72
RODSF [35]	33.23	30.89	26.21	*21.85*	18.28	25.62	24.51	*22.31*	*19.00*	16.37
LRODF$_{m=3}$	**34.76**	*32.07*	*26.76*	*21.96*	*18.13*	**27.67**	**25.70**	*22.55*	*19.25*	16.61
LROD-AMF$_{m=3}$	*33.88*	*32.01*	25.04	19.85	16.89	*27.22*	*24.95*	21.75	17.63	15.86
LROD-PMF$_{m=3}$	*33.87*	**32.10**	26.07	19.88	16.92	*27.23*	*24.97*	21.77	17.65	15.89
LRODF$_{m=4}$	*33.81*	31.36	**26.87**	**22.94**	*18.82*	*26.41*	*25.13*	**22.57**	**19.47**	*16.77*
LROD-AMF$_{m=4}$	33.27	31.56	*26.39*	21.57	*18.86*	24.61	23.58	20.92	18.21	*16.88*
LROD-PMF$_{m=4}$	33.25	*31.67*	*26.45*	21.63	**18.93**	24.62	23.60	20.94	18.22	**16.91**

Table 6 Performance comparison in terms of CMSSIM (10^{-1}) using the Peppers and Parrots detail images contaminated with different probabilities p of impulsive noise

P	Peppers					Parrots				
	0.1	0.2	0.4	0.6	0.8	0.1	0.2	0.4	0.6	0.8
VMF [2]	9.78	9.83	9.32	*8.33*	*5.58*	9.90	*9.79*	*9.40*	*7.88*	**5.26**
IPGSAMF [19]	9.02	8.19	5.88	3.87	3.00	9.05	8.08	6.29	4.83	3.12
FIVF [17]	9.89	9.84	8.39	5.78	3.14	9.57	9.04	8.24	5.54	2.99
AVMF [12]	9.90	9.44	7.07	3.78	2.46	9.62	9.11	6.69	3.72	2.27
PGSAMF [20]	9.86	9.81	8.08	4.61	2.12	9.82	9.23	7.57	3.98	2.08
RODSF [35]	9.93	9.95	8.83	*7.29*	*4.55*	*9.94*	9.58	8.66	6.64	*4.24*
LRODF$_{m=3}$	*9.98*	*9.98*	*9.38*	*7.99*	*5.06*	**9.98**	*9.77*	9.25	7.04	*4.39*
LROD-AMF$_{m=3}$	**10.00**	*9.98*	9.33	6.57	3.06	*9.95*	9.75	9.11	6.62	3.24
LROD-PMF$_{m=3}$	*9.99*	*9.98*	*9.35*	6.58	3.07	*9.95*	*9.76*	9.14	6.63	3.27
LRODF$_{m=4}$	*9.98*	**9.99**	**9.52**	**8.43**	**5.62**	**9.98**	**9.84**	**9.44**	**7.95**	*5.25*
LROD-AMF$_{m=4}$	*9.99*	*9.97*	*9.39*	6.79	3.37	*9.94*	9.70	*9.28*	*7.28*	3.68
LROD-PMF$_{m=4}$	*9.99*	*9.97*	*9.39*	6.79	3.37	*9.94*	9.71	*9.33*	*7.30*	3.68

the range $[d_{\min}, d_{\max}] = [80, 200]$ when $m = 4$. The values $d_T = 75$ and $d_T = 130$ have been selected as sub-optimal for $m = 3$ and $m = 4$ respectively. As can be seen in Figs. 5*c* and *d*, the optimal value d_{Topt} moves towards the end of the range for low noise intensities, and moves towards the beginning of the range for high intensities. Consequently, a second sub-optimal value of d_T can be defined by using a linear interpolation in the range $[d_{\min}, d_{\max}]$ as follows

$$d_T = d_{\min} + p'(d_{\max} - d_{\min}) \tag{5}$$

where p' is the probability of detecting a noisy pixel. Although the exact amount of noise is generally unknown, a visual assessment

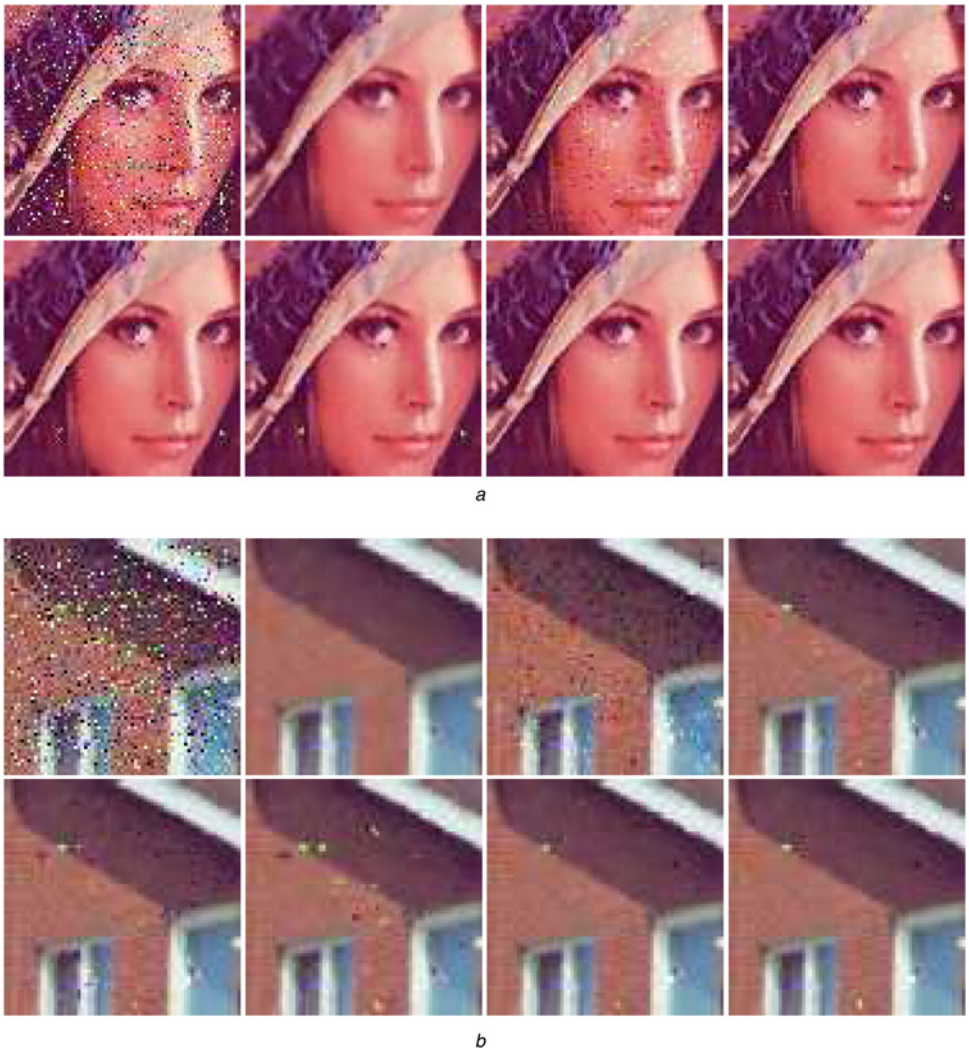

Fig. 6 *From left- to right-hand side and from top to bottom: original image, and images filtered with VMF, IPGSAMF, FIVF, AVMF, PGSAMF, RODSF and LRODS-VMF for the*

a Lenna detail image with p = 0.2 of impulsive noise.
b House detail image with p = 0.3 of impulsive noise.

IET Image Process., 2016, Vol. 10, Iss. 1, pp. 24–33

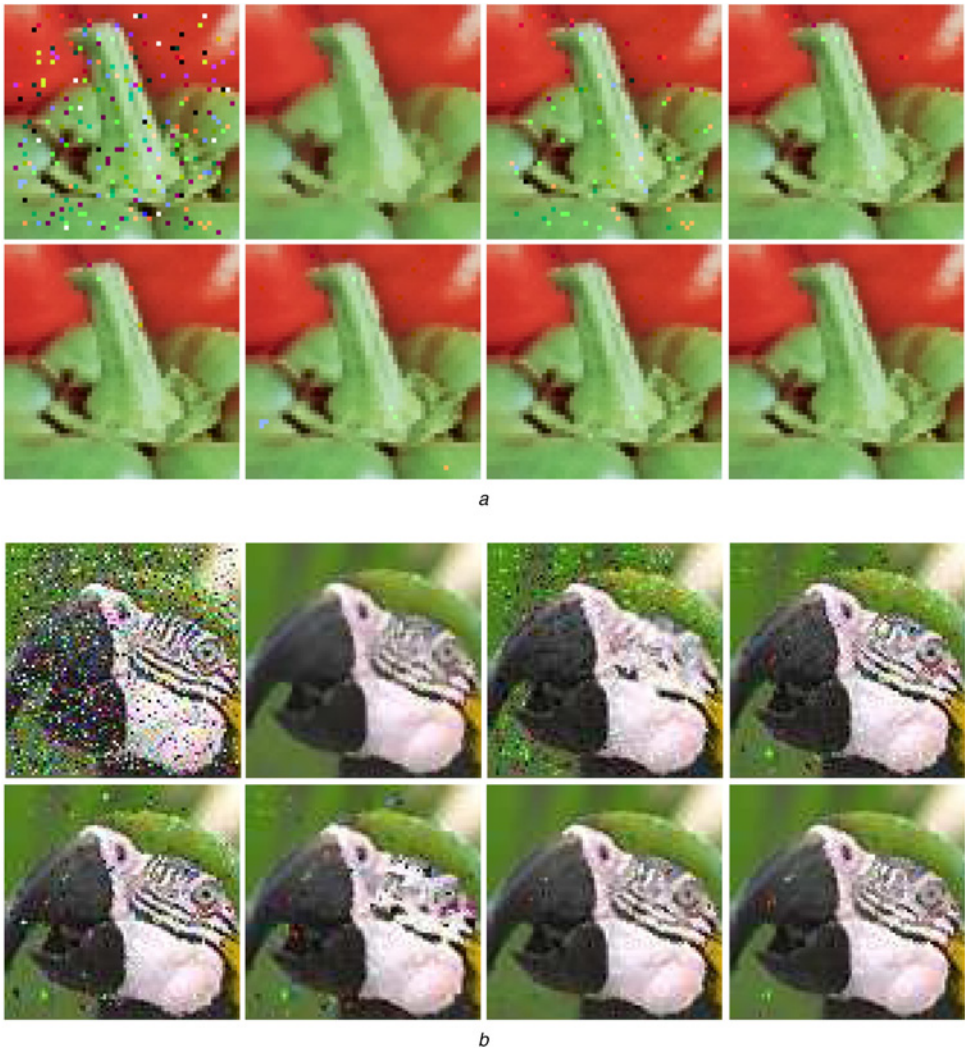

Fig. 7 *Results for the*

a Peppers
b Parrots detail images with $p = 0.1$ and $p = 0.4$ impulsive noise respectively. From left- to right-hand side and from top to bottom: original image, and images filtered with VMF, IPGSAMF, FIVF, AVMF, PGSAMF, RODSF and LRODS-VMF

can be made, or an estimate can be made by examining the ratio p' between noisy pixels detected with the first suboptimal value of d_T and the total number of pixels. As we have seen in the previous section, p' is a good approximation of the real probability of noise p. One approach is initially choose the first suboptimal value of d_T and, if more precision is needed, use the second suboptimal value defined by (5).

To assess the proposed LRODF method, its behaviour was compared with several classic as well as more recent filters, namely: VMF, iterative peer group switching arithmetic mean filter (IPGSAMF) [19], fast impulsive vector filter (FIVF) [17], adaptive vector median filter (AVMF) [12], peer group switching arithmetic mean filter (PGSAMF) [20], and RODSF [35]. We present the results for the zoomed Lenna and Parrots images. Similar behaviour is obtained for the other images.

Tables 1–6 show that LRODF obtained the best overall results in terms of PSNR, NCD, and CMSSIM meaning that LRODF presents the best balance between noise reduction and signal preservation. Although it was proposed to use the VMF filter on pixels detected as corrupted, the results are also shown with AMF, PMF, and using $m = 3$ and $m = 4$, to do a more complete comparison.

From a visual analysis of the outputted images (Figs. 6 and 7) it can be seen that LRODF has a similar ability to VMF (which is the most robust method) to reduce noise. It can also be seen that LRODF exceeds the noise reduction capacity of other filters while retaining edges and details as seen in the figures and in the CMSSIM tables. The only downside to this and other switching filters is that in the case of high noise levels, a group of noisy pixels can be considered as a detail to be retained – as in the image filtered with LRODS-VMF in Fig. 7*b*.

The results obtained show that the developed method reveals good properties in visual perception (NCD), noise reduction capabilities (PSNR) and similarity in luminance, contrast and structure (CMSSIM), and is robust when impulsive noise increases. Good performance is also obtained using AMF and PFM – even with high levels of impulsive noise. Consequently, given its robustness, it is proposed to generally use LRODF with $m = 4$.

We also check the efficiency of the LRODF on 50 images [Complete results available at http://personales.upv.es/broig/images/LRODF/LRODFreport.pdf], and obtained the values presented in Table 7. Fixing a quantity of impulsive noise ($p =$ 0.1, 0.2, 0.4, 0.6, 0.8) and a quality mesure (NCD, PSNR, CSSIM), we define N_1 as the number of times a filter has the best quality measure value and N_3 as the number of times a filter is in the three top positions. Table 7 shows the percentages $100(N_1/50)$ on the left-hand side side, and $100(N_3/3^{\cdot 50})$ on the right-hand side. It can be seen that most times LRODF is in the first position and that it also has the best performance when we take into account the top three best values for the three quality measures.

Table 7 Percentage of cases in which a filter is in the first position or in the top three positions for the different quality measures when applied to 50 images

p	% in 1st, position					% in 1st, 2nd or 3rd position				
	0.1	0.2	0.4	0.6	0.8	0.1	0.2	0.4	0.6	0.8
NCD										
VMF	0	0	*2*	*4*	*40*	0	0	6	26.7	30.7
IPGSAMF	0	0	0	*0*	*0*	0	0	0.7	0.7	0
FIVF	0	0	0	0	*0*	0	0	0	0	0
AVMF	2	0	0	0	0	2.7	0.7	0	0	0
PGSAMF	0	0	0	0	0	0	0	0	0	0
RODSF	*4*	0	0	0	0	*9.3*	*10.7*	*8.7*	*14*	*17.3*
LRODF$_{m=3}$	**50**	*34*	0	0	0	**30.7**	**29.3**	*19.3*	*20.6*	*12*
LROD-AMF$_{m=3}$	*6*	*4*	0	0	0	*12*	6	1.3	0	0.6
LROD-PMF$_{m=3}$	*18*	*12*	*2*	0	0	*20.7*	*12.7*	0.7	0	0
LRODF$_{m=4}$	*18*	**46**	**88**	**92**	**52**	*20*	*27.3*	**31.3**	**32.7**	**32.7**
LROD-AMF$_{m=4}$	2	*2*	*4*	*2*	0	1.3	3.3	*12*	2	2.7
LROD-PMF$_{m=4}$	0	2	*4*	*2*	*8*	3.3	*10*	*20*	*3.3*	*4*
PSNR										
VMF	*0*	0	*0*	*18*	**48**	0.7	0.7	*14.7*	*29.3*	**28.7**
IPGSAMF	0	0	*0*	*0*	*0*	0	0	0.7	0.7	0
FIVF	0	0	0	0	0	0	0	0	0	0
AVMF	0	0	0	0	0	0	0	0	0	0
PGSAMF	0	0	0	0	0	0	0	0	0	0
RODSF	*4*	*2*	0	0	0	*7.3*	*12*	*13.3*	*8.7*	*2.7*
LRODF$_{m=3}$	**54**	*18*	0	0	0	**30.7**	*27.3*	4.6	2	1.3
LROD-AMF$_{m=3}$	0	0	0	0	*2*	*12.7*	2.7	0.7	0	0.6
LROD-PMF$_{m=3}$	*20*	*4*	*2*	0	0	*23.3*	*10*	0.7	0.7	1.3
LRODF$_{m=4}$	*22*	**74**	**86**	**72**	*18*	*20.7*	**30.7**	**32**	**31.3**	*24.7*
LROD-AMF$_{m=4}$	0	0	0	*2*	0	1.3	5.3	*13.3*	*4.6*	*12*
LROD-PMF$_{m=4}$	0	*2*	*12*	*8*	*32*	3.3	*11.3*	*20*	*22.7*	**28.7**
CSSIM										
VMF	0	0	*0*	*8*	*30*	2	*9.3*	*21.3*	*29.3*	*30.7*
IPGSAMF	0	0	*0*	*0*	*0*	0	0	0	0.7	0.7
FIVF	0	0	0	0	*0*	0.7	0	0	0	0
AVMF	*4*	0	0	0	0	4	0	0	0	0
PGSAMF	0	0	0	0	0	0	0	0	0	0
RODSF	4	*4*	0	0	0	*11.3*	*9.3*	*8.7*	*6*	*18*
LRODF$_{m=3}$	**34**	*18*	0	0	0	**28.7**	*28*	*20.7*	*24.7*	*15.3*
LROD-AMF$_{m=3}$	4	*6*	0	0	0	*10.6*	6	1.3	0	0
LROD-PMF$_{m=3}$	*14*	2	0	0	0	*12.7*	*6.7*	0	0	0
LRODF$_{m=4}$	*34*	**62**	**90**	**88**	**66**	*20.7*	**28.7**	**32.7**	**32.7**	**32.7**
LROD-AMF$_{m=4}$	*6*	*8*	*8*	*2*	0	5.3	5.3	7.3	2	*1.3*
LROD-PMF$_{m=4}$	0	0	*2*	*2*	*4*	4	6.7	*8*	*4.6*	1.3

5 Conclusions

In this paper, a good statistic for detecting impulsive noise in colour images is presented. A new geometric localisation algorithm on a 5×5 window is presented that is robust against increases in impulsive noise and able to retain details of fine lines and edges. It divides the 5×5 window in nine 3×3 subwindows containing the central pixel and computes the ROD$_m$ statistic with $m = 4$ over each subwindow. If there are at least three subwindows with small ROD$_m$ then the pixel is considered not corrupt.

From this statistic, an alternating filter is proposed that is applied on pixels marked as noisy. The VMF is performed on these pixels. Different options have been studied before defining an optimal configuration for the filter obtaining, in general, the computational complexity lower than the VMF. Experimental results show that the proposed method has competitive performance and can efficiently reduce impulsive noise in colour images while retaining edges and details.

6 References

1 Tukey, J.W.: 'Nonlinear (nonsuperposable) methods for smoothing data'. Proc. Congr. Rec. EASCOM, 1974, vol. 74, pp. 673–681
2 Astola, J., Haavisto, P., Neuvo, Y.: 'Vector median filters', *Proc. IEEE.*, 1990, **78**, pp. 678–689
3 Lukac, R., Smolka, B., Martin, K., *et al.*: 'Vector filtering for color imaging', *IEEE Signal Process. Mag., Special Issue on Color Image Processing*, 2005, **22**, pp. 74–86
4 Lukac, R., Plataniotis, K.N.: 'A taxonomy of color image filtering and enhancement solutions', in Hawkes, P.W. (Ed.): 'Advances in imaging and electron physics' (Elsevier, 2006), vol. 140, pp. 187–264
5 Plataniotis, K.N., Venetsanopoulos, A.N.: 'Color Image processing and applications' (Springer-Verlag, 2000)
6 Allende, H., Galbiati, J.: 'A non-parametric filter for image restoration using cluster analysis', *Pattern Recognit. Lett.*, 2004, **25**, pp. 841–847
7 Alajlan, N., Kamel, M., Jernigan, E.: 'Detail preserving impulsive noise removal', *Signal Process Image Commun.*, 2004, **19**, pp. 993–1003
8 Ng, P.E., Ma, K.K.: 'A switching median filter with boundary discriminative noise detection for extremely corrupted images', *IEEE Trans. Image Process.*, 2006, **15**, pp. 1506–1516
9 Jin, L., Li, D.: 'An efficient color impulse detector and its application to color images', *IEEE Signal Process. Lett.*, 2007, **14**, pp. 397–400
10 Lin, T.C., Yu, P.T.: 'Partition fuzzy median filter based on fuzzy rules for image restoration', *Fuzzy Sets Syst.*, 2004, **147**, pp. 75–97
11 Schulte, S., De Witte, V., Nachtegael, M., *et al.*: 'Fuzzy random impulsive noise reduction method', *Fuzzy Sets Syst.*, 2007, **158**, pp. 270–283
12 Lukac, R., Plataniotis, K.N., Venetsanopoulos, A.N., *et al.*: 'A statistically-switched adaptive vector median filter', *J. Intell. Robot. Syst.*, 2005, **42**, pp. 361–391
13 Srinivasan, K.S., Ebenezer, D.: 'A new fast and efficient decision-based algorithm for removal of high-density impulse noises', *IEEE Signal Process. Lett.*, 2007, **14**, pp. 189–192
14 Chan, R.H., Chung-Wa, H., Nikolova, M.: 'Salt-and-pepper noise removal by median-type noise detectors and detail-preserving regularization', *IEEE Trans. Image Process.*, 2005, **14**, pp. 1479–1485
15 Gallegos-Funes, F.J., Ponomaryov, V.: 'Real-time image filtering scheme based on robust estimators in presence of impulse noise', *Real-Time Imaging*, 2004, **10**, pp. 69–80
16 Lukac, R.: 'Adaptive color image filtering based on center weighted vector directional filters', *Multidimens. Syst. Signal Process.*, 2004, **15**, pp. 169–196
17 Morillas, S., Gregori, V., Peris-Fajarnés, G., *et al.*: 'A fast impulsive noise color image filter using fuzzy metrics', *Real-Time Imaging*, 2005, **11**, pp. 417–428
18 Smolka, B., Lukac, R., Chydzinski, A., *et al.*: 'Fast adaptive similarity based impulsive noise reduction filter', *Real-Time Imaging, Special Issue on Spectral Imaging*, 2003, **9**, pp. 261–276
19 Morillas, S.: 'Fuzzy metrics and peer groups for impulsive noise reduction in color images'. Proc. 14th European Signal Processing Conf. EUSIPCO2006, Florence, Italy, 2006
20 Smolka, B., Chydzinski, A.: 'Fast detection and impulsive noise removal in color images', *Real-Time Imaging*, 2005, **11**, pp. 389–402

21 Dong, Y., Xu, S.: 'A new directional weighted median filter for removal of random-valued impulse noise', *IEEE Signal Process. Lett.*, 2007, **14**, pp. 193–196
22 Jin, L., Li, D.: 'A switching vector median filter based on the CIELAB color space for color image restoration', *Signal Process.*, 2007, **87**, pp. 1345–1354
23 Yuan, S.Q., Tan, Y.H.: 'Impulse noise removal by a global-local noise detector and adaptive median filter', *Signal Process.*, 2006, **86**, pp. 2123–2128
24 Garnett, R., Huegerich, T., Chui, C., *et al*.: 'A universal noise removal algorithm with an impulse detector', *IEEE Trans. Image Process.*, 2005, **14**, pp. 1747–1754
25 Shen, Y., Barner, K.E.: 'Fast adaptive optimization of weighted vector median filters', *IEEE Trans. Signal Process.*, 2006, **54**, pp. 2497–2510
26 Lukac, R., Plataniotis, K.N., Smolka, B., *et al*.: 'cDNA microarray image processing using fuzzy vector filtering framework', *Fuzzy Sets Syst. Special Issue on Fuzzy Sets and Systems in Bioinformatics*, 2005, **152**, pp. 17–35
27 Nie, Y., Barner, K.E.: 'The fuzzy transformation and its application in image processing', *IEEE Trans. Image Process.*, 2006, **15**, pp. 910–927
28 Yuksel, M.E.: 'A hybrid neuro-fuzzy for edge preserving restoration of images corrupted by impulse noise', *IEEE Trans. Image Process.*, 2006, **15**, pp. 928–936
29 Hanji, G., Latte, M.V.: 'Detail preserving fast median based filter', *J. Adv. Comput. Sci. Technol.*, 2012, **1**, (4), pp. 195–206
30 Ibrahim, H., Kong, N.S.P., Ng, T.F.: 'Simple adaptive median filter for the removal of impulse noise from highly corrupted images', *IEEE Trans. Consum. Electron.*, 2008, **54**, (4), pp. 1920–1927
31 Suganthi, A., Senthilmurugan, M.: 'Comparative study of various impulse noise reduction techniques', *Int. J. Eng. Res. Appl.*, 2013, **3**, (5), pp. 1302–1306
32 Varghese, J.: 'Adaptive switching rank-ordered impulse noise filters: new techniques, results, and analysis', *Int. J. Imaging Sci. Eng.*, 2007, **1**, (2), pp. 52–59
33 Gonzalez, R.C., Woods, R.E.: 'Digital image processing' (Addison Wesley, 1992)
34 Perona, P., Malik, J.: 'Scale-space and edge detection using anisotropic diffusion', *PAMI*, 1990, **12**, pp. 629–639
35 Peris-Fajarnés, G., Roig, B., Vidal, A.: 'Rank-ordered differences statistic based switching vector filter', *LNCS*, 2006, **4141**, pp. 74–81
36 Aubert, G., Kornprobst, P.: 'Mathematical problems in image processing' (Springer, 2006)
37 Weickert, J.: 'Coherence-enhancing diffusion filtering', *Int. J. Comput. Vis.*, 1999, **31**, pp. 111–127
38 Hassan, M., Bhagvati, C.: 'Structural similarity measure for color images', *Int. J. Comput. Appl.*, 2012, **43**, (14), pp. 7–12